Wake analysis of coastal wind turbines in GRASP on the Dutch shoreline

M. Dirksen[1,*], M. Rijntalder[2,*], P. Baas[3,*], I.L. Wijnant[4,*]

Mekelweg 5, 2628CD Delft, the Netherlands

January 11, 2023

Abstract

Wind turbines extract energy from the flow. As a result, downstream of wind turbines the wind speed is reduced. This is called a wake effect. In this report we analyse the wake effects for the coastal Eemshaven wind turbine site in two steps:

- Validate the high resolution (100x100x25m) large eddy simulation model GRASP on a 25.6x25.6x2.2km domain centred around the Eemshaven wind turbine site using measurements from three nearby lidars (Yard, Oudeschip and Strekdammen). The validation period covers August 2020 until December 2020. We distinguish GRASP-CTL (control) and GRASP-ADM (Actuator Disk Model) and compare them to the lidar measurements. GRASP-ADM shows a clear improvement compared with GRASP-CTL.
- Use the normalized difference between validated GRASP-CTL and GRASP-ADM to build a wake detection model that follows the wakes downstream. We find wakes 94% of the time. Velocity deficits as high as 40% at a distance of 500m from the wind turbines were found.

Keywords: Wind farm wake effect, LES, GRASP, Actuator Disk Parametrization, The Netherlands, Lidar

*Corresponding author

Email address: mariekedirksen@gmail.com (M. Dirksen)

[1]Delft University of Technology (TUD), PO Box 5, 2600 AA Delft, The Netherlands

[2]Pondera, Amsterdamseweg 13, 6814CM Arnhem, the Netherlands

[3]Whiffle, Molengraaffsingel 8, 2629JD Delft, the Netherlands

[4]KNMI, Utrechtseweg 297, 3731GA de Bilt, the Netherlands

1. Introduction

In October 2022 the installed wind energy capacity in the Netherlands was 8,304MW of which about 70% onshore. Most onshore wind turbines are located near the shore. The number and size of wind farms are expected to grow rapidly in the next decade, especially offshore. According to the latest plans of the Dutch government, offshore wind energy will be the Dutch main power supply in 2030 with 21GW installed capacity. More and bigger wind farms imply larger power losses due to wake and blockage effects caused by those wind farms. Wind farm wakes can be observed more than 50km from a wind farm, both onshore (Lundquist et al., 2019) and offshore (Cañadillas et al., 2020), which means that in the future many wind farms will experience power losses due to wake effects of upstream located wind farms. Therefore it is of the utmost importance that we understand those effects and are able to model them.

We distinguish between in-farm wake modelling where the actual wake generation by the wind turbines takes place and what happens outside the wind farm where wake decay is determined by the atmospheric conditions. Most engineering wake models that are used by the wind energy industry are of limited use for modelling wake decay behind wind farms. One of the most advanced engineering wake models (TurbOPark (Nygaard et al., 2020)) allows for non-uniform inflow into the wind farm due to wake effects from upstream wind farms, but it does not take into account spatial gradients in the flow, stability or wake curvature. However, as wind farms get larger, it becomes more and more important to take these effects into account in combination with realistic atmospheric inflow conditions. Wake decay and curvature behind wind farms can be successfully modelled with mesoscale models using a Wind Farm Parametrisation (WFP) (Stratum et al., 2019; Fischereit et al., 2021). However, for sites with significant local changes in surface roughness, such as coastal areas, the resolution of the current mesoscale models (1-3km) is too coarse (see Appendix B).

In contrast, Large Eddy Simulation (LES) models, which run on high resolutions like 100m and finer, can resolve processes on the 1-3km scales (Maas and Raasch, 2022; Eriksson et al., 2017; Hasager et al., 2015; Jiménez et al., 2015). As such, we expect LES models to outperform mesoscale models on local atmospheric effects relevant for wake propagation. Because LES

simulations are typically done on a much smaller domains than mesoscale models they cannot handle far-wakes. As the domain in this study is limited to 25.6x25.6km, we can only analyse wakes up to the domain edge.

In order to analyse the near farm wakes behind the Eemshaven wind turbines we used GPU-Resident Atmospheric Simulation Platform (GRASP) simulations with and without Actuator Disk Parametrisation (ADM): GRASP-CTL and GRASP-ADM. Using a method similar to (Krutova et al., 2021) we classified the wake structures based on the normalized differences between the GRASP-CTL and GRASP-ADM.

The goal of this report is to analyse the wake characteristics of wind turbines at a complex site for weather and wake modelling. For this analyses we built a wake detection model based on the wind speed from the LES model GRASP. The Eemshaven site with a 220MW turbine capacity is ideal for this study, not only because the site is on the coast, but also because there are three lidar measurement campaigns nearby that can be used for validation of GRASP (at 500m, 715m and 2.1km from the wind turbines). GRASP is run on a 100m by 100m horizontal grid spacing and for a 5 month period from August until December 2020. The research questions of this report are:

- Q1: How does GRASP validate against the lidar measurements?
- Q2: What are the wake characteristics of the Eemshaven wind turbines, considering wake intensity, frequency and length?

nn The outline of the report is as follows. The methodology is described in section 2 and includes information about the lidar data used for the model validation, the GRASP settings and the wake detection algorithm. The validation results are described in section 3 and the modelled wake characteristics in section 4. Section 5 and 6 summarize the conclusions provide suggestions for future research.

2. Methodology

2.1. Site description

The wind turbine site of Eemshaven is in located the northeastern part of the Netherlands. The wind turbines are positioned on the shoreline. There are six different turbine types at the Eemshaven site and their turbine specific characteristics are individually modelled in GRASP. The hub height of the

different turbines varies from 93 to 132m and the rotor diameter from 82 to 136m. The cut-in wind speed ranges from 2.5 to 4 m/s. An overview of the site is provided in Fig. 1.

Three lidars measuring campaigns have been performed near the Eemshaven wind turbine site: one on the western border of the wind turbine site (the Yard location, disturbed by the wind turbines between 93-160^o), one on the northern border of the wind turbine site (the Strekdammen location, disturbed by the wind turbines between 92-320^o) and one south of the wind turbine site (the Oudeschip location, disturbed between 266-125^o). The Strekdammen and Yard lidars are closest to the wind turbines with a minimum distance of respectively 500m and 715m to the nearest wind turbine. The Oudeschip lidar is not on the coast and further from the nearest wind turbine (2.1 km).

The measurements were performed with two Zephir300 lidars in the period August to December 2020. The Strekdammen lidar has measured the entire 5 month measuring period with a data availability of 95%. The Yard and Oudeschip both cover two months, with a data availability of respectively 98% and 96%. The Yard lidar measured from August until the beginning of October when it was moved to the location Oudeschip.

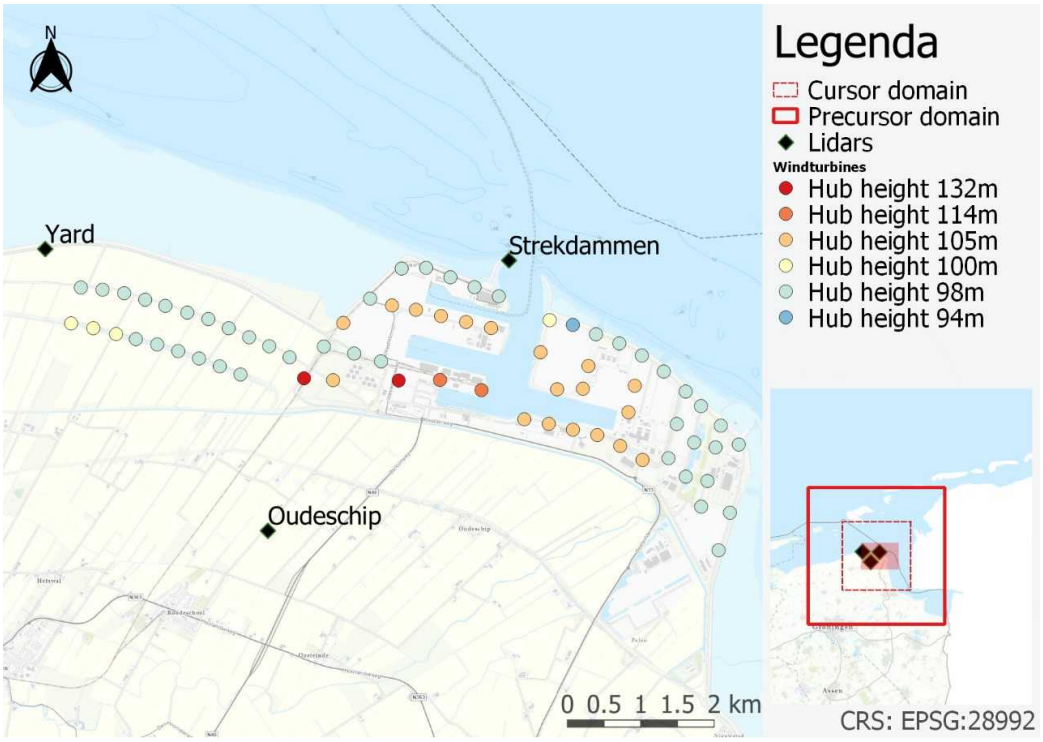

Figure 1: LiDAR and wind turbine locations of Eemshaven and the domain of the GRASP run. In the bottom right figure the solid red line shows the precursor domain, the dashed line the cursor domain and the shaded area highlights the wind turbine area (shown in the left figure).

2.2. Model description

The GPU-Resident Atmospheric Simulation Platform (GRASP) is a Large Eddy Simulation model that performs its core routines on Graphics Processing Units (GPUs) (Schalkwijk et al., 2012). Using GPUs allows the simulation to be much faster, thus reducing the large computational costs traditionally associated with LES.

DALES. GRASP is based on Dutch Atmospheric Large Eddy Simulation (DALES), which is still widely used in the atmospheric boundary layer community. The basic LES equations that GRASP uses are the same as in DALES and are extensively described in Heus et al. (2010).

TESSEL. Just like in DALES, GRASP uses the TESSEL land surface model which has been developed by the European Centre for Medium Range Weather

Forecasting (ECMWF) (ECMWF, 2017). Over land, momentum, heat and moisture exchange between the atmosphere and the soil depend on vegetation type. Over sea, air-sea momentum exchange is described using a simple Charnock relation which assumes that the drag coefficient continuously increases with the wind speed because higher winds cause higher surface roughness (in this study α_{CH} is 0.0185 for all simulations).

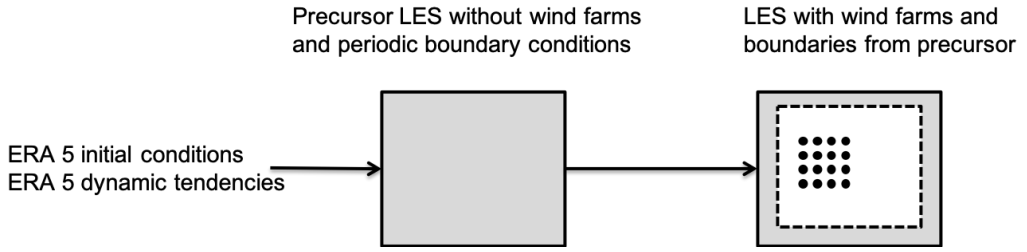

Figure 2: Schematic representation of the LES model setup. ERA5 fields are used to estimate the initial conditions and are applied as dynamic tendencies to a pre-cursor LES with periodic boundary conditions. The pre-cursor LES values (a simulation without wind turbines) are to prevent the wakes from re-entering the domain.

Lateral boundary conditions. For the present study we run GRASP with periodic lateral boundary conditions. The large-scale forcings are prescribed as tendencies to the model equations, i.e. the state variables contain an extra forcing term to account for the large-scale processes (Schalkwijk et al., 2015; Neggers et al., 2012). The large-scale tendencies are derived from ECMWFs ERA5 reanalysis dataset. For heating or cooling due to radiation, the radiation computations are done offline based on ERA5 data and subsequently prescribed as tendencies during runtime. To avoid the recirculation of wakes, we make use of a concurrent pre-cursor simulation (Stevens et al., 2014). This is a simulation without wind turbines that runs in parallel with the actual simulation. Over the boundary region the values of the actual simulation are strongly nudged towards the precursor simulation. The specifics of the pre-cursor simulations are given In Appendix A.

Actuator Disk Model. Wind turbines are modeled using the Actuator Disk Model (ADM) described by (Meyers and Meneveau, 2010). The required input for this parametrisation (power curve, thrust curve, rotor diameter and hub height) is described in section 2.1. The ADM calculates the drag forces (using the thrust curve) and rotational forces (using the power curve) based

on local wind speed, taking the actual induction into account. Individual yaw control based on the local wind direction is applied to the turbines.

2.3. Wake detection algorithm

The wake detection algorithm that we used is an adapted version of the algorithm described in (Krutova et al., 2021). The three main differences are: (1) In (Krutova et al., 2021) the free flow is assumed to be equal to the flow outside the wake, whereas in our method we take the free flow in the wake from GRASP-CTL. (2) In Krutova et al. (2021) the centreline is defined as the middle of the wake area, whereas we follow the path of the strongest wake effect. This implies that our method can deal with non-symmetrical wake intensities whereas (Krutova et al., 2021) assume a symmetrical wake intensity. (3) In (Krutova et al., 2021) the radius of the circular detection zone increases moving "down-wake", whereas in our method we used a circular buffer around each new wake centre (masking the upstream wake area). This means the algorithm runs more efficiently, especially for longer wakes.

The wake detection algorithm is based on the wind speed difference between GRASP-CTL and GRASP-ADM at a height of 100m. GRASP-ADM is effectively GRASP-CTL including the Actuator Disk Parametrisation (ADM) described in section 2.2. The wind speeds from GRASP are inversely normalized, with a value of 0 for the highest wind speeds and 1 for the lowest wind speeds. The inverse normalized wind speed (I) is calculated as follows:

$$I_{ij} = \frac{U_{max} - U_{ij}}{U_{max} - U_{min}} \tag{1}$$

Where U_{max} is the maximum wind speed in the full 25.6x25.6km domain, U_{min} the minimum wind speed in the domain and U_{ij} the wind speed at location ij. The threshold value Tr for wake detection is defined as:

$$Tr_{ij} = \frac{U_{max} - 0.95U_{ref,ij}}{U_{max} - U_{min}} \tag{2}$$

Where $U_{ref,ij}$ is the reference wind speed from GRASP-CTL at location ij. So the threshold for wake detection is set at 95% of the GRASP-CTL wind speed. For a point at location ij to be considered part of the wake, U_{ij} should be lower than 0.95 $U_{ref,ij}$ (in other words: I_{ij} should be higher than Tr_{ij}). However, if I_{ij} is higher than Tr_{ij} it does not automatically

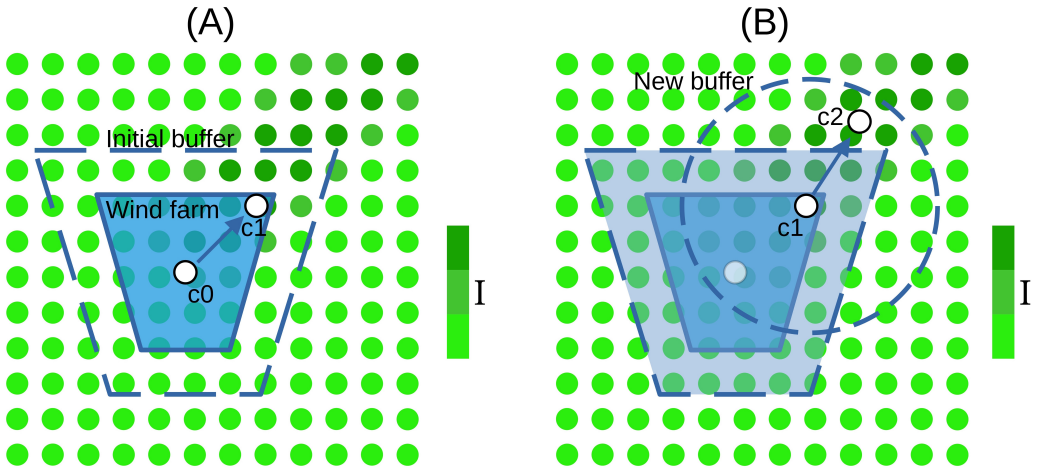

Figure 3: Schematic illustration of the wake detection. (A) In the background the wake intensity of the grid points in green. From the centre of the wind farm (c0) a initial buffer zone is drawn. Within the initial buffer zone the weighted averaged new centre c1 is calculated. (B) From c1 a new circular buffer is drawn with the initial buffer radius (and increased if necessary). Similarly the next centre c2 is calculated, following the centre lines of the wake.

mean the point is classified as part of the wake. Only points attached to the Eemshaven wind turbine site can.

Figure 3 illustrates how the wake detection algorithm works. To make sure that only points attached to the wind turbine site are considered as part of the wake, we start the wake detection from the centre of the wind turbine site and define a buffer zone depending on the size of the wind turbine site A_{WF} (or rather $\frac{\sqrt{A_{WF}}}{\pi}$). Within the wind turbine site and buffer zone the points where I_{ij} is higher than Tr_{ij} are classified as part of the wake.

The next step in the wake detection algorithm is that the point in the buffer zone with the highest wake intensity is calculated. This point is the new centre point of the wake. So, the centre point of the wake becomes the point where the wake is strongest. This is different from the definition of (Krutova et al., 2021) where the centre is defined as the middle of the wake shape.

From the new centre point a circular buffer area is drawn with a the same initial radius. Areas that have been classified as part of the wake in previous steps of the wake detection algorithm are excluded from the buffer zone. In case not enough points remain in the buffer zone (less than 500) or all points

in the buffer zone classify as wake points, the radius of the buffer zone is increased with 3km.

The wake detection moves downstream until there are no more points where U_{ij} is lower than 0.95 $U_{ref,ij}$ (or I_{ij} higher than Tr_{ij}) or the wake centre point does no longer move. It is possible that there are points outside the buffer zones where the wind speed in GRASP-ADM is less than 95% of the wind speed in GRASP-CTL without these points being part of the wake. The difference can be a result of small phase differences between GRASP-ADM and GRASP-CTL. These points are removed at the end of the wake detection by detecting outlier clusters, i.e. detected areas which are not attached to the main wake from the wind turbine site. This also implies we neglect detecting broken wake structures.

From the detected wake structures we have calculated the normalized velocity deficit at various distances from the centre of the wind turbine site. Surrounding the wind turbine site a line with distances from 500m up to 6000m from the wind turbines was drawn. The velocity in the detected wake polygons within a 100m buffer from these lines was averaged.

3. GRASP validation at Oudeschip, Strekdammen and Yard

There are a total of 138 distinct days available between 2020-07-31 and 2020-12-14 for the validation. The 10 minute wind speeds from GRASP were directly compared with the 10 minute averaged wind speeds from the lidars. Figure 4 shows the directional wind speed and wind profile for each lidar location, averaged over the validation period. The wind speed was averaged for each 15^o wind direction sector. The wind profiles are included from 60-220m. The uncertainty of the lidar wind measurements below 50m and above 220m is too high. The averaged profile and the 0.3-0.7 quantile interval is shown.

At the Yard lidar site (Fig. 4A), which is west of the Eemshaven wind turbines, only the east/southeastern winds are disturbed (the disturbed wind directions are indicated with the red bar). The GRASP-CTL and GRASP-ADM wind speeds from the undisturbed wind directions are similar and closely agree with the lidar measurements. In the disturbed wind direction sector GRASP-ADM models a clear wake effect (1.5 m/s lower wind speeds than GRASP-CTL). The observed wind speeds rather follow the course of the GRASP-CTL wind speed. This suggests that in reality the wake effect is smaller than in GRASP-ADM, despite the close proximity of the wind turbines. Further research is needed to determine the cause of this discrepancy. For instance, apart from modelling errors, it could be that wind turbines were not in operation during part of the measurement campaign. The mean wind profile of Yard generally shows an overestimation of the GRASP-CTL wind speed while GRASP-ADM is in closer agreement with the measurements.

At the Strekdammen lidar site (Fig. 4B) we observe a clear improvement by using GRASP-ADM instead of GRASP-CTL: for the disturbed wind directions there is a much better agreement between the lidar measurements and GRASP-ADM than with GRASP-CTL (note that the modelled wake effect of around 1.5 m/s is rather similar to the wake effect modeled at the Yard location). The same improvement is observed for all measurement heights (see the wind profiles). For this location the wind turbines have a clear impact on the mean, omni-directional wind speed profile. Below hub height GRASP-ADM gives a slightly higher spread in wind speed compared to the measurements, but this is mostly within the 0.3m/s measurement uncertainty. As to be expected, GRASP-CTL shows the largest overestimations around hub height.

At the Oudeschip lidar site (Fig. 4C) there are not enough disturbed

measurements to draw robust conclusions. Both in the wind direction sector averaged values as in the wind profiles the differences between the two GRASP runs and the measurements are small. However, GRASP seems to underestimate the higher wind speeds with about 0.5m/s (the 0.7 quantile).

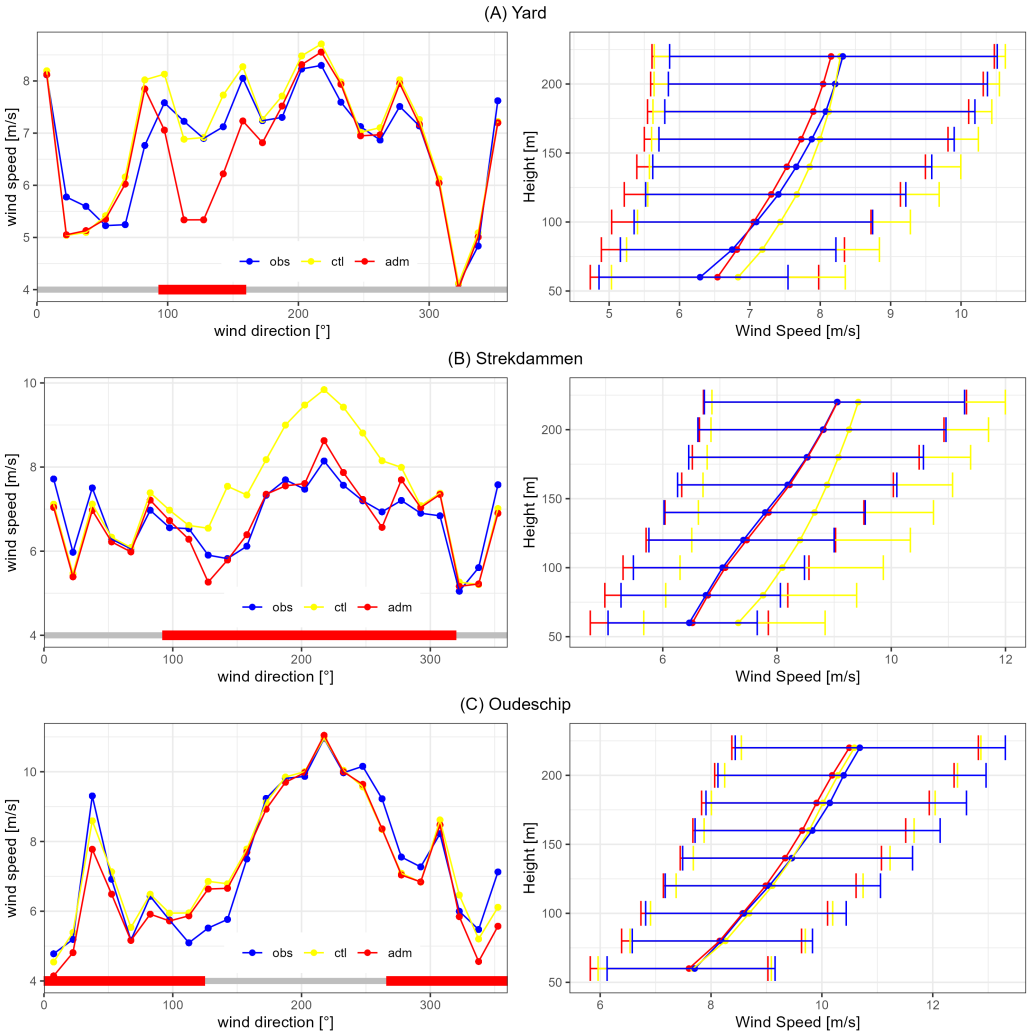

Figure 4: Directional wind speeds around hub height (100m) and wind profiles averaged over the validation period. The profiles are shown for the lidar locations (A) Yard, (B) Strekdammen and (C) Oudeschip. For the directional figures the wind speed was averaged over a 15 degrees wind direction sector. The red bar indicates the disturbed wind direction. The blue, yellow and red lines are the lidar measurements, GRASP-CTL and GRASP-ADM, respectively. For the wind profiles the same color coding has been applied. The lines are the averaged values and the bars show the 0.3-0.7 quantile intervals.

4. Wake characteristics

Figure 5 shows an averaged velocity deficit (GRASP-ADM minus GRASP-CTL) for northeasterly (Fig. 5A), southeasterly (Fig. 5B), southwesterly (Fig. 5C) and northwesterly (Fig. 5D) winds around hub height (100m). The predominant wind direction is southwesterly. The wind direction selection is based on GRASP-CTL at lidar site Oudeschip. The largest wake deficits are within the wind turbine site (up to 2.5m/s). Outside the wind turbine site we find averaged velocity deficits up to 1.5m/s.

On average the wake structures seem to be within the GRASP domain. When considering individual cases however, 62% of the wakes were longer than the shortest distance from the center of the domain to the domain edge (13.2km). Here we assumed the wake length to be from the centre of the Eemshaven wind turbine site up the furthest detected wake point, but the length from the centre to the edge of the wind turbine site is not equal for all wind directions. So, for future research the definition of the wake length should be improved. The edge of the wind turbine site can be determined based on the wind direction and can be used for the definition of the wake length instead of the centre of the turbine site.

Figure 6 shows the wake frequency at a height of 100m in the GRASP modelling domain. There are almost always wakes within the Eemshaven turbine site (94% of the hours in the 4 month validation period). With prevailing southwesterly winds, wakes more frequently occur north of the turbine site. At about 2km from the turbine site there are still wakes about half of the time. Only looking at the west-northwesterly winds the wakes are obviously to the east of the turbine site and seem to be effected by the domain edge. We do not observe this for south-southwesterly winds (with almost 3 times as many cases). We observe a clear blockage pattern for south-southwesterly winds, but none for west-northwesterly winds. This is probably because of the shape of the wind turbine site: significantly wider from the north and south.

Figure 7 shows the relative velocity deficits (calculated using equation 1 for GRASP-CTL and GRASP-ADM and taking the difference) up to 6km from the Eemshaven wind turbines for different wind speeds classes. For some turbines the first class 0-4m/s is below the cut-in wind speed. This is also why there are hardly any wakes within this wind speed class.

The largest normalized velocity deficit and spread are observed for wind speeds between 4-10m/s. In the second wind speed class 4-7m/s the aver-

aged wind speed deficit decreases from 20% at 500m to 12% at 6km from the wind turbine site. However, the 0.9 quantile shows that wind speeds were even 40% lower at a distance of 500m. Above 10m/s we observe less spread and a smaller averaged normalized velocity deficit. This is as expected because at higher wind speeds wakes are generally less pronounced because the atmosphere is less often stable (Dirksen et al., 2022).

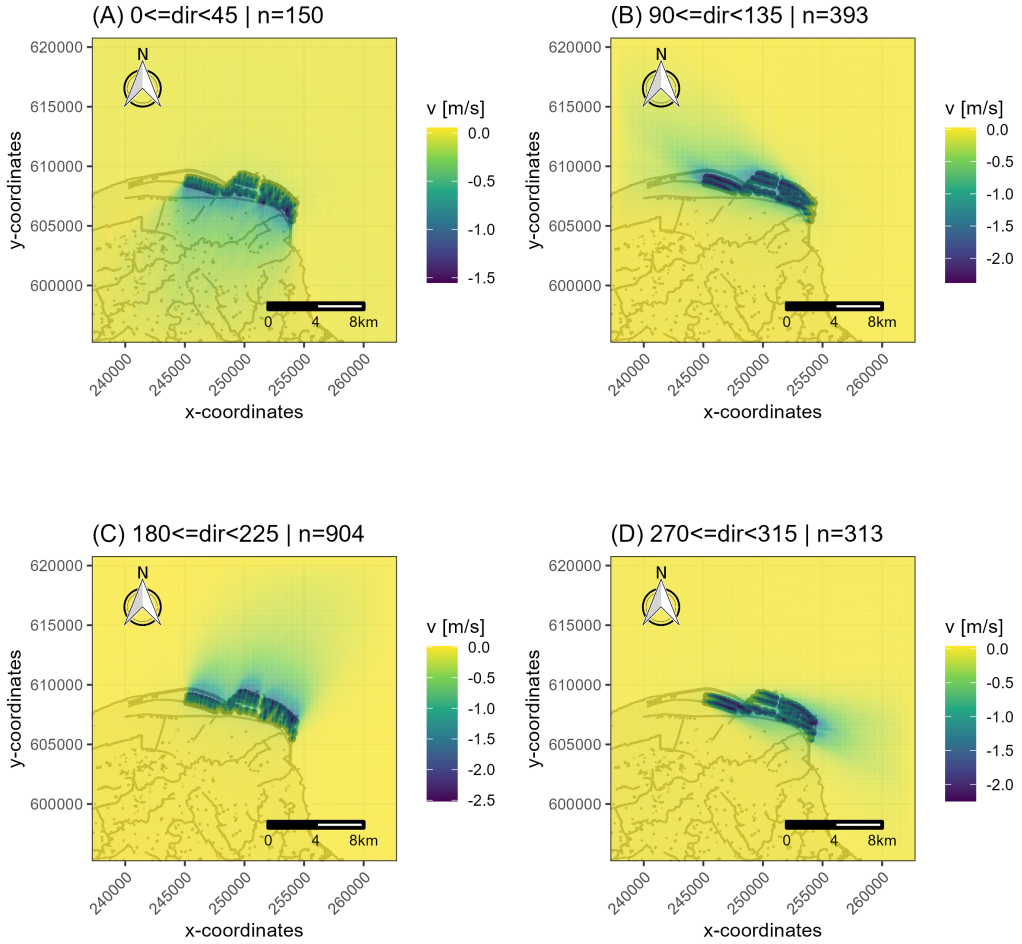

Figure 5: Velocity deficit at a height of 100m (GRASP-ADM minus GRASP-CTL) in the GRASP modelling domain for wind direction sectors at lidar site Oudeschip: (A) northeasterly, (B) southeasterly, (C) southwesterly and (D) northwesterly wind directions. n denotes the number of wind fields from GRASP. Only the hourly wind fields during the validation period August-December 2020 were used for the averaged images.

(a)

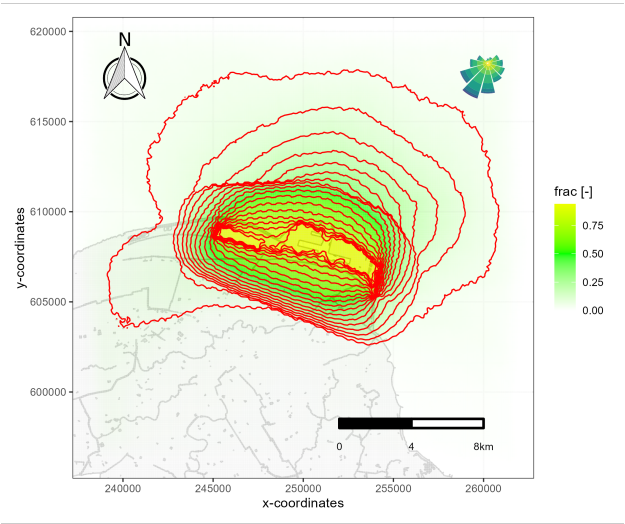

(b) (c)

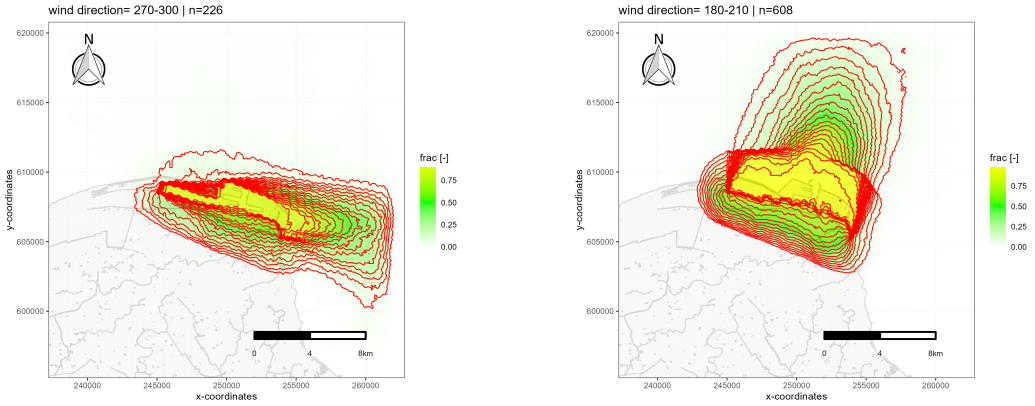

Figure 6: Frequency of the detected wakes at a height of 100m in the GRASP-ADM on a scale from 0 to 1. (a) The frequency of the wakes is defined by the GRASP-ADM wake hours divided by the total number of hours in the validation period. The red lines mark every 5% interval. The maximum wake frequency of 94% is within the Eemshaven wind turbine site. The wind rose in the top right corner of the plot shows that the predominant wind direction is southwesterly. (b) shows the wake frequency for west-northwesterly winds and (c) for south-southwesterly winds.

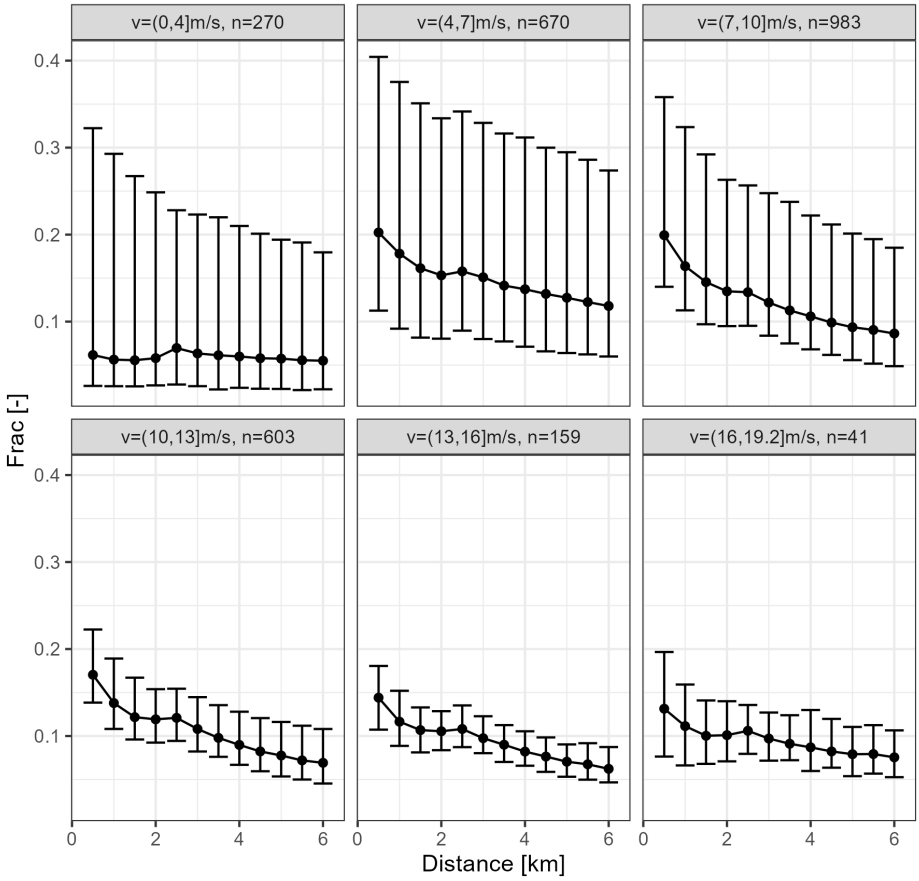

Figure 7: Normalized velocity deficit or fraction at a height of 100m (calculated using equation 1 for GRASP-CTL and GRASP-ADM and taking the difference) for six different wind speed classes: 0-4m/s (for some turbines below cut-in wind speed), 4-7m/s, 7-10m/s, 10-13m/s, 13-16m/s and 16-19.2m/s (for most turbines at rated power). n denotes the number of cases in each class. The distance to the edge of the turbine site is on the x-axis (from 500m to 6km in steps of 500m). The bars indicate the 0.1-0.9 quantile interval.

5. Conclusions

The goal of this report is to assess how the wind turbines at Eemshaven affect the wind speed inside and outside the turbine site, especially downwind from the wind turbines (the wake). A wake detection model was built in order to be able to quantify the wake (shape, length) for analyses (e.g. to assess wake frequency) based on Large Eddie Simulations (LES) with the GRASP model with (GRASP-ADM) and without (GRASP-CTL) the effects of wind turbines on the atmosphere.

Q1: How does GRASP validate against the lidar measurements?
The GRASP model had a horizontal resolution of 100x100m. The GRASP wind speeds have been validated at three lidar locations. GRASP model output from the grid cells closest to these locations was compared with the 10 minute averaged lidar measurements. Especially at the Strekdammen lidar site, on the edge of the wind turbines field, we see a clear improvement of the actuator disk model compared with the control run (without wind farm effects). At the Yard lidar site we did not find an improvement. More research is needed to determine the cause of the observed discrepancy between model and observations. At the Oudeschip lidar site, which is located at a larger distance from the wind turbines, the modelled wake effect is small. From the available observations it is not possible to draw robust conclusions on the performance of the turbine parameterization for this location.

Q2: What are the wake characteristics of the Eemshaven wind turbines, considering wake intensity, frequency and length?
The wake characteristics have been analysed using a wake detection method similar to the one developed/used by (Krutova et al., 2021). Using the normalized wind speeds a wake threshold has been defined, based the difference between the runs with and without wind farm effects.

The velocity deficits around hub height (100m) in the Eemshaven wind turbine site, averaged over the validation period August-December 2020, were up to 2.5m/s. Outside the turbine site the averaged velocity deficits were locally as large as 1.5m/s. Following the wakes downstream we find the largest normalized velocity deficits for wind speeds between 4-10m/s. At a distance of 500m from the turbine site we find deficits around 20%. This is still around 10% at a distance of 6km.

Within the wind turbine area, wakes have been detected 94% of the time.

Around 3km from the farm the wake frequency had decreased to about 50%. Evidently, with prevailing southwesterly winds northeasterly wake structures are more common. When considering individual cases however, 62% of the wakes were longer than the shortest distance from the center of the domain to the domain edge (13.2km).

6. Future research

The wake detection relies on the normalized difference between GRASP-CTL and GRASP-ADM. Hereby we assumed that the only difference between the two simulations is the actuator disk model. Although by eye the noise factor seems to be small we aim at quantifying the noise objectively in future research.

Currently the detected wakes are a single area. For future research we aim at classifying at least three different areas: (1) blockage area, (2) initialization phase of the wake in the wind turbine site and (3) wake behind the wind turbines. For different wind directions we will then be able to quantify characteristics of each individual area rather than the entire wake. For example, the stability can be significantly different for each area, also considering land/sea transitions. With a southern wind the blockage area will be positioned over land while the wakes behind the turbines are above sea.

Appendices

A. Sensitivity of the model settings

A typical GRASP simulation has a precursor and a cursor run (see also 2), both runs require a simulation domain and a resolution. Settings are determined following a trade-off between computational costs and desired accuracy. The domain and resolution of precursor and cursor run do not have to match, hence three settings are tested in this GRASP study.

To test the sensitivity of the domain and resolution for the (pre)cursor run, three settings are analysed for a small period of time, i.e. a sensitivity run of 10 days. For these sensitivity runs, a selection of representative wind days is made, which includes various wind speeds and wind directions. The sensitivity settings can be found in 1.

Table 2 shows the validation results of the sensitivity runs at the lidar locations Oudeschip, Yard and Strekdammen. GRASP run 1, with a resolution of 100x100m and a single precursor domain, has the largest bias. Increasing the resolution to 66m (GRASP run 2) shows a small improvement of the bias, at Yard the bias was reduced from -0.43m/s to -0.23m/s. Alternatively to increasing the resolution GRASP run 3 uses a double precursor. The validation results are similar to GRASP run 2, though computationally less expensive.

Run	Precursor		Cursor	
	Domain (km x km)	Resolution (m x m x m)	Domain (km x km)	Resolution (m x m x m)
1	25.6 x 25.6	100 x 100 x 25	25.6 x 25.6	100 x 100 x 25
2	25.6 x 25.6	66.7 x 66.7 x 25	25.6 x 25.6	66.7 x 66.7 x 25
3	50 x 50	200 x 200 x 25	25.6 x 25.6	100 x 100 x 25

Table 1: Tested GRASP settings for the different sensitivity runs. The model runs with GRASP start every day at 00:00.

Table 2: Validation of the GRASP settings for resolutions and precursor domain. The sensitivity runs covered a period of 10 days.

	bias Oudeschip	bias Strekdammen	bias Yard	RMSE Oudeschip	RMSE Strekdammen	RMSE Yard	R^2 Oudeschip	R^2 Strekdammen	R^2 Yard
GRASP run 1	-0.77	-0.41	-0.43	1.65	1.50	1.62	0.86	0.83	0.80
GRASP run 2	-0.67	-0.39	-0.24	1.77	1.38	1.38	0.62	0.85	0.83
GRASP run 3	-0.76	-0.33	-0.23	1.79	1.37	1.29	0.63	0.85	0.85

B. Comparison with HARMONIE

In addition to the validation of GRASP-ADM with measurements we have also compared GRASP-ADM with the modelling results from the NWP model HARMONIE. The data from the WINS50 project (Wijnant et al., 2022), HARMONIE cycle 43 with the wind farm parametrisation of (Fitch et al., 2012), covers the our validation period.

For the comparison with the HARMONIE data the lidar and GRASP data were first processed. The HARMONIE data has a resolution of 2.5 by 2.5km. In order to match the difference in spatial scale the GRASP and lidar wind speeds were averaged around the hour of the instantaneous HARMONIE wind speed.

Comparing the overall performance there seems to be a small preference for GRASP, which has an hourly averaged bias of 0.1m/s or less. The bias of HARMONIE is within 0.3m/s. The squared correlation coefficient is slightly higher for GRASP at all lidar locations. Also the RMSE is lower for GRASP, both models have the smallest squared correlation coefficient and RMSE at the Yard location.

Table 3: Validation of the GRASP wind speed at the lidar locations Oudeschip, Strekdammen and Yard compared with HARMONIE wind. The GRASP and lidar wind speeds were averaged around the hour of the instantaneous HARMONIE wind speed to match the difference in spatial scale.

stn	count	measurements	GRASP	HARMONIE	bias GRASP	bias HARMONIE	R^2 GRASP	R^2 HARMONIE	RMSE GRASP	RMSE HARMONIE
Oudeschip	13570	9.40	9.30	9.09	-0.10	-0.31	0.89	0.85	1.29	1.53
Strekdammen	26839	7.82	7.87	7.70	0.05	-0.12	0.88	0.83	1.29	1.47
Yard	13862	7.51	7.44	7.63	-0.07	0.13	0.84	0.80	1.43	1.62

References

B. Cañadillas, R. Foreman, V. Barth, S. Siedersleben, A. Lampert, A. Platis, B. Djath, J. SchulzStellenfleth, J. Bange, S. Emeis, and T. Neumann. Offshore wind farm wake recovery: Airborne measurements and its representation in engineering models. *Wind Energy*, 23(5):1249–1265, may 2020. ISSN 1095-4244. doi: 10.1002/we.2484. URL `https://onlinelibrary.wiley.com/doi/abs/10.1002/we.2484`.

M. Dirksen, I. Wijnant, A. P. Siebesma, P. Baas, and N. E. Theeuwes. Validation of wind farm parameterisation in Weather Forecast Model HARMONIE-AROME. Technical report, TU Delft, Delft, 2022. URL `https://www.wins50.nl/publications/`.

ECMWF. Ifs manual part iv: Physical processes. *IFS Documentation Cy43R3. Technical report, ECMWF*, 2017.

O. Eriksson, M. Baltscheffsky, S. P. Breton, S. Söderberg, and S. Ivanell. The Long distance wake behind Horns Rev I studied using large eddy simulations and a wind turbine parameterization in WRF. *Journal of Physics: Conference Series*, 854(1), jun 2017. ISSN 17426596. doi: 10.1088/1742-6596/854/1/012012.

J. Fischereit, R. Brown, X. G. Larsén, J. Badger, and G. Hawkes. Review of Mesoscale Wind-Farm Parametrizations and Their Ap-

plications. *Boundary-Layer Meteorology*, 2021. ISSN 0006-8314. doi: 10.1007/s10546-021-00652-y. URL https://doi.org/10.1007/s10546-021-00652-y.

A. C. Fitch, J. B. Olson, J. K. Lundquist, J. Dudhia, A. K. Gupta, J. Michalakes, and I. Barstad. Local and mesoscale impacts of wind farms as parameterized in a mesoscale NWP model. *Monthly Weather Review*, 140 (9):3017–3038, 2012. ISSN 00270644. doi: 10.1175/MWR-D-11-00352.1.

C. B. Hasager, P. Vincent, R. Husson, A. Mouche, M. Badger, A. Peña, P. Volker, J. Badger, A. Di Bella, A. Palomares, E. Cantero, and P. M. Correia. Comparing satellite SAR and wind farm wake models. In *Journal of Physics: Conference Series*, volume 625. Institute of Physics Publishing, jun 2015. doi: 10.1088/1742-6596/625/1/012035.

T. Heus, C. C. van Heerwaarden, H. J. J. Jonker, A. Pier Siebesma, S. Axelsen, K. van den Dries, O. Geoffroy, A. F. Moene, D. Pino, S. R. de Roode, and J. Vilà-Guerau de Arellano. Formulation of the dutch atmospheric large-eddy simulation (dales) and overview of its applications. *Geoscientific Model Development*, 3(2):415–444, 2010. doi: 10.5194/gmd-3-415-2010. URL https://gmd.copernicus.org/articles/3/415/2010/.

P. A. Jiménez, J. Navarro, A. M. Palomares, and J. Dudhia. Mesoscale modeling of offshore wind turbine wakes at the wind farm resolving scale: a composite-based analysis with the Weather Research and Forecasting model over Horns Rev. *Wind Energy*, 18(3):559–566, mar 2015. ISSN 10954244. doi: 10.1002/we.1708. URL http://doi.wiley.com/10.1002/we.1708.

M. Krutova, M. Bakhoday-Paskyabi, J. Reuder, and F. G. Nielsen. Development of an image processing method for wake meandering studies and its application on data sets from scanning wind lidar and large-eddy simulation. *Wind Energy Science*, Discuss [p(September):1–34, 2021.

J. K. Lundquist, K. K. DuVivier, D. Kaffine, and J. M. Tomaszewski. Costs and consequences of wind turbine wake effects arising from uncoordinated wind energy development. *Nature Energy 2019*, 4(1): 26–34, nov 2019. ISSN 2058-7546. doi: 10.1038/S41560-018-0281-2. URL https://www-nature-com.tudelft.idm.oclc.org/articles/s41560-018-0281-2.

O. Maas and S. Raasch. Wake properties and power output of very large wind farms for different meteorological conditions and turbine spacings: A large-eddy simulation case study for the German Bight. *Wind Energy Science*, 7(2):715–739, mar 2022. ISSN 23667451. doi: 10.5194/wes-7-715-2022.

J. Meyers and C. Meneveau. Large eddy simulations of large wind-turbine arrays in the atmospheric boundary layer. *48th AIAA Aerospace Sciences Meeting Including the New Horizons Forum and Aerospace Exposition*, (January):1–10, 2010.

R. A. J. Neggers, A. P. Siebesma, and T. Heus. Continuous single-column model evaluation at a permanent meteorological supersite. *Bulletin of the American Meteorological Society*, 93(9):13891400, 2012.

N. G. Nygaard, S. T. Steen, L. Poulsen, and J. G. Pedersen. Modelling cluster wakes and wind farm blockage. *Journal of Physics: Conference Series*, 1618(6), sep 2020. ISSN 17426596. doi: 10.1088/1742-6596/1618/6/062072.

J. Schalkwijk, E. Griffith, F. Post, and H. Jonker. High performance simulations of turbulent clouds on a desktop pc. *Bulletin of The American Meteorological Society*, 93(3):307–314, 2012. ISSN 0003-0007. doi: 10.1175/BAMS-D-11-00059.1.

J. Schalkwijk, H. J. J. Jonker, A. P. Siebesma, and F. C. Bosveld. A year-long large-eddy simulation of the weather over cabauw: an overview. *Monthly Weather Review*, 143:828844, 2015.

R. J. Stevens, J. Graham, and C. Meneveau. A concurrent precursor inflow method for large eddy simulations and applications to finite length wind farms. *Renewable Energy*, 68:4650, 2014.

B. Stratum, S. Basu, I. L. Wijnant, J. Barkmeijer, J. Onvlee, and A. P. Siebesma. Wind turbine parametrisation in HARMONIE-AROME. pages 1–28, 2019. URL `https://www.dutchoffshorewindatlas.nl/publications/reports/2019/12/06/knmi-report---wind-turbine-parameterisation`.

I. L. Wijnant, N. Theeuwes, B. Van Ulft, T. Zoer, and P. Baas. Wind farms in WINS50 climatology. 2022. URL `https://wins50.nl/downloads/wind_farms_in_wins50_climatology.pdf`.